

Phase Crossover induced by Dynamical Many Body Localization in Periodically Driven Long-Range Spin Systems

Mahbub Rahaman,¹ Takashi Mori,² and Analabha Roy¹

¹Department of Physics, The University of Burdwan, Golapbag, Bardhaman - 713 104, India

²RIKEN CEMS, 2-1 Hirosawa, Wako, Saitama, 351-0198, Japan

Dynamical many-body freezing occurs in periodic transverse field-driven integrable quantum spin systems. Under resonance conditions, quantum dynamics causes practically infinite hysteresis in the drive response, maintaining its starting value. We extended this to non-integrable many body systems by reducing the Hamiltonian symmetries through a power-law dependence in spin exchange energy, $J_{ij} = 1/|i - j|^\beta$. The dynamics of the integrable short-range Transverse Field Ising Model (TFIM) and non-integrable long-range Lipkin Meshkov-Glick (LMG) models were investigated. In the LMG, the resonance conditions in the driving field suppresses the heating postulated by the *Eigenstate Thermalization Hypothesis* (ETH) by inducing *Dynamical Many Body Localization*, or DMBL. This is in contrast to Many Body Localization (MBL), which requires disorder to suppress ETH. DMBL has been validated by the Inverse Participation Ratio (IPR) of the quasi-stationary Floquet modes. While TFIM has IPR localization for all drive parameters, the LMG exhibits high-frequency localization only at the resonances. IPR localization in the LMG deteriorates with an inverse system size law at lower frequencies, which indicates heating to infinite temperature. Furthermore, adiabatically increasing frequency and amplitude from low values raises the Floquet state IPR in the LMG from nearly zero to unity, indicating a phase crossover. This occurrence enables a future technique to construct an MBL engine in clean systems that can be cycled by adjusting drive parameters only.

Keywords: Dynamical localization, Thermalization, Phase Crossover

Periodically driven Quantum Many Body Systems can, under certain conditions, experience Dynamical Many-Body Freezing (DMF) when dynamical hysteresis stops observables from reaching their diagonal averaged values and thermalizing to infinite temperature [1–3].

Under certain resonance conditions in the drive parameters, DMF can cause the response to ‘freeze’ completely to its initial value at all times. This arises as a consequence of additional approximate symmetries that occur at resonance. DMF has been demonstrated via the Rotating Wave Approximation (RWA) in the driven TFIM with nearest-neighbour interactions [4] and is shown to be protected when translational invariance is explicitly broken (say, by disorder) [5, 6].

The utilization of Floquet theory simplifies the analysis of time-periodic systems. For closed quantum systems governed by the time-dependent Schrödinger equation, the *Floquet Hamiltonian* allows for a mapping of the time-dependent dynamics into the dynamics of a time-independent effective Hamiltonian, provided the system is strobed at integer multiples of the time period of the drive. The time independent eigenstates of the effective Hamiltonian correspond to quasi-stationary *Floquet Modes* of the original Hamiltonian. The temporal progression of the system comes from phase coefficients that capture the dynamics [7, 8].

Any sufficiently complex non-integrable Many Body System is expected to thermalize according to the

Eigenstate Thermalization Hypothesis (ETH) despite the fact that closed quantum dynamics preserves the memory of the initial state of the system. This arises due to the properties of the matrix elements of observables in typical states[9]. The ETH can be readily adapted to time-periodic systems using Floquet theory (the Floquet-ETH, or FETH). Nonetheless, the conditions for ETH to hold are not particularly strong, and the density matrix of the system can fail to approach one that is described by a thermal expression. In such cases, the system is said to undergo *Many Body Localization* (MBL) Thermal systems must conduct because they exchange energy and particles internally during thermalization. Thus, insulating systems can be naturally athermal; Many Body Localization is a well-studied case [10]. This phenomenon is stable against local perturbations, and constitutes an exotic state of matter with far-reaching implications in theoretical physics, as well as in practical applications[11].

The addition of disorder has been identified as a crucial component in the onset of MBL. In that case, thermalization is prevented by disorder-induced localization. Nonetheless, alternative approaches to MBL in strongly interacting disorder-free systems [12–14], inhomogeneous systems [15–18], and by inducing disorder in the emergent physics [19] and by other effective means [17] (albeit with strong finite-size effects), have been reported. An alternative approach to realizing MBL in disorder-free homogeneous many-body systems involve *Floquet Engineering*, where a time-

See an-
notation.

periodic drive is introduced, and the drive parameters tuned to introduce a clustering of quasistationary energies in a manner similar to localization[9].

In this article, we propose that additional approximate symmetries can be Floquet engineered in quantum many body systems with lower symmetry than the TFIM, such as those with long-range interactions. We use the fact that emergent approximate symmetries can be engineered in Floquet systems and apply it to long-range interactions. This results in both DMF and MBL occurring simultaneously at resonant values of the drive parameters, and complete thermal behaviour at other values. This phenomenon is distinct from DMF in the TFIM, since clean TFIM systems, being integrable, never thermalize..

See annotation

To demonstrate the onset of MBL, we investigate the driven Lipkin-Meshkov-Glick (LMG) model[20–25], a long-range system that extends the nearest neighbour interactions in the TFIM to all-to-all interactions. [26–28] that is a special case of the more general Curie-Weiss model, wherein the nearest neighbour exchange in the TFIM is extended to longer ranges with a power law dependence, $J_{ij} \sim 1/|i-j|^\beta$. Setting $\beta = \infty$ recovers the TFIM, and setting $\beta = 0$ yields the LMG model. We have recovered the onset of DMF in this system and have supported our result with numerical simulations.

In addition, we compare the degree of localization of the quasi-stationary Floquet modes in both limits of β in the LMG model with the TFIM. In order to do so, we look at the Inverse Participation Ratio (IPR) of the Floquet modes in the representation given by the eigenstates of the symmetry-breaking field. The IPR, closely related to the concept of quantum purity, is defined as the formal sum of the square of the density in some physically meaningful space or representation. A high IPR of a stationary state denotes low participation in most of the representation, and a low IPR distributes participation uniformly across the representation, leading to ergodic dynamics[29]. Thus, IPR [30] is a useful tool for witnessing MBL of a quantum system. For an MBL system, the IPR is unity, and it scales inversely with the system size number of spins when it is thermally distributed [31].

In the first section of this paper, we present all essential theoretical frameworks. Our results for the LMG model are presented next in section II. In that section, we have used the Rotating Wave Approximation (RWA) [32], where only the slowest rotating terms in the Fourier expansion of the Hamiltonian in a frame co-rotating with the symmetry breaking drive field are retained. In addition, we have the obtained analytical expressions for numerical simulations of the Floquet modes and their IPR. They are used to probe the system dynamics in the high and low-frequency

domains at both limits of β . In section III we have used phase space plots to contrast the low and high frequency limits of the LMG model in the thermodynamic limit by mapping it to an equivalent classical Hamiltonian system. Finally, in section IV, we have looked at numerical computations of the IPR of the Floquet modes for different values of the drive parameters, well beyond those that allow for the RWA. We observed that, if the system is driven by an adiabatically increasing drive frequency from low to high limit while remaining in the resonance region, a sharp crossover from a thermal to an MBL phase occurs. We conclude with discussions and outlook.

I. BACKGROUND

The Eigenstate Thermalization Hypothesis (ETH) is a series of conjectures that allows for the thermalization of an isolated quantum many body system. The state of the system, $|\psi(t)\rangle$, evolves according to the Schrödinger equation $\hat{H}|\psi(t)\rangle = i\frac{\partial}{\partial t}|\psi\rangle$. The Hamiltonian \hat{H} is assumed to be *non-integrable*, in that it lacks an extensive number of *local* additive conserved quantities, that is to say, there are no set of observables \hat{O}_s such that $\hat{H} = \sum_s \hat{O}_s$ for any extensive index s . It lacks an extensive number of conserved quantities that can be written as a sum of local operators, that is to say, there are no set of observables $\hat{O}_s = \sum_i \hat{L}_i$ such that $[\hat{O}_s, \hat{H}] = 0$. Here, the \hat{O}_s constitute an arbitrary CSCO (complete set of commuting observables), and \hat{L}_i are *local*, each having sub-extensive support in the system [33]. In addition, we postulate the existence of an equivalent Hamiltonian \hat{H}_{eq} for every Hamiltonian \hat{H} as well as an "equilibrium" value A_{eq} for every observable \hat{A} , such that

$$A_{eq}(E) \equiv \frac{\text{Tr}(\hat{A}e^{-\beta\hat{H}_{eq}})}{\text{Tr}(e^{-\beta\hat{H}_{eq}})}, \quad (1)$$

where $E = \langle\psi(t)|\hat{H}|\psi(t)\rangle$ is the conserved energy of the system, and $\beta = 1/(k_B T)$ is the inverse temperature, H_{eq} is an effective Hamiltonian that captures the long-time average dynamics of the system, and k_B is the Boltzmann constant.

To put it simply, ETH proposes that this many-body Hamiltonian undergoes thermalization as seen in the *long-time averages* of observables, with the eigenstates bearing resemblance to thermal states. The aforementioned hypothesis serves as a valuable instrument for comprehending the conduct of stimulated quantum systems and their correlation with thermal equilibrium. This assertion can be justified

by examining the expectation value of an observable \hat{A} as it evolves under the Schrödinger equation. To see this, we first expand the state of the system $|\psi(t)\rangle$ as:

$$|\psi(t)\rangle = \sum_m c_m(t) |m(0)\rangle,$$

where $|m(0)\rangle$ represents the eigenstates of $\hat{H}(0)$ with energy E_m . The coefficients $c_m(t)$ describe the time-dependent amplitude of the expansion. Plugging these expansions into the expression for the expectation value, we obtain the long-time average of the expectation value [34]:

$$\overline{\langle \hat{A}(t) \rangle} = \sum_{m,k} \overline{c_m^*(t)c_k(t)} \langle m(0)|\hat{A}|k(0)\rangle, \quad (2)$$

where the overline indicates the following operation for any time-dependent quantity $\mathcal{O}(t)$,

$$\overline{\mathcal{O}} \equiv \lim_{t \rightarrow \infty} \frac{1}{t} \int_0^t d\tau \mathcal{O}(\tau). \quad (3)$$

Had the system been integrable, the large number of conserved quantities would restrict mixing between the states during unitary evolution. In the non-integrable case, the system explores the entire Hilbert space spanned by eigenstates with eigenvalues close to E more or less uniformly. In that case, the matrix elements $\langle m(0)|\hat{A}|k(0)\rangle$ are said to satisfy the Srednicki ansatz [35, 36]:

$$\langle m(0)|\hat{A}|k(0)\rangle \approx A_{eq} \left(\frac{E_m + E_k}{2} \right) \delta_{mk} + e^{-\frac{1}{2}S\left(\frac{E_m+E_k}{2}\right)} f\left(\frac{E_m + E_k}{2}, E_m - E_k\right) R_{mk}. \quad (4)$$

Here, S is the thermodynamic entropy and R_{mk} are elements of a random matrix with vanishing mean and unit variance. What this means for the ensuing dynamics is that the system explores the accessible Hilbert space uniformly, and the matrix elements $\langle m(0)|\hat{A}(t)|k(0)\rangle$ become indistinguishable for most pairs of m and k . Applying this ansatz and taking the thermodynamic limit by ignoring terms $\mathcal{O}(e^{-S/2})$, the expression for the expectation value becomes:

$$\begin{aligned} \overline{\langle \hat{A}(t) \rangle} &\approx \sum_m \overline{|c_m(t)|^2} A_{eq}(E_m) \\ &\approx A_{eq}(E) \sum_m \overline{|c_m(t)|^2} = A_{eq}(E), \end{aligned}$$

where, in the last step, we utilized the fact that A_{eq} is a smooth function, and that the states with energies far from E have $|c_m(t)|^2 \approx 0$. Therefore, in the limit of large systems the expectation value of an observable

\hat{A} is approximately equal to the thermal expectation value A_{eq} . This is the essence of the ETH, which suggests that individual eigenstates of a quantum system can be described by statistical mechanics in the long-time limit.

We now generalize the ETH to non-integrable many-body systems that are closed, but not isolated. In that case, it is possible to impart a periodic time-dependence on the Hamiltonian while still ensuring unitary evolution. If the time period of the drive is T , and the corresponding drive frequency $\omega \equiv 2\pi/T$, the Floquet theorem states that the solutions to the Schrödinger equation can be written as $|\psi(t)\rangle = e^{-i\epsilon t/\hbar} |\phi(t)\rangle$, where the $|\phi(t)\rangle$ are T -periodic states called *Floquet Modes*, the corresponding $\epsilon \in \mathbb{R}$, are called *quasienergies*. Quasienergy values are not unique, and can be made to be bounded within a Floquet photon Brillouin zone, viz. a range $[-\omega/2, \omega/2]$ [37, 38]. As a consequence, the unitary evolution operator can be split into two parts as follows [39].

$$U(t) = e^{-i\hat{K}_F(t)} e^{-i\hat{H}_F t}. \quad (5)$$

Here, the micromotion operator $\hat{K}_F(t)$ is time-periodic in T , with $\hat{K}_F(0) = 0$, and the Floquet Hamiltonian $\hat{H}_F = \hat{H}(t) - i\frac{\partial}{\partial t}|_{t=T}$

$$\hat{H}_F = e^{i\hat{K}_F(t)} [\hat{H}(t) - i\partial_t] e^{-i\hat{K}_F(t)}. \quad \text{Thus, if the system is strobed at integer multiples of } T \text{ only, then the unitary evolution matches that of a time independent Hamiltonian } H_F. \quad (6)$$

In such systems, the Floquet Eigenstate Thermalization Hypothesis (FETH) posits that, subject to specific conditions and in the context of a system of significant size, the Floquet modes themselves exhibit thermal state-like behavior, i.e., $\hat{H}_{eq} \approx \hat{H}_F$ in eqn 1. However, in contrast to the isolated systems, the loss of energy conservation allows for the mixing of all Floquet modes in the ensuing dynamics, not just those with quasienergies near E . Were this to actually happen in the ensuing dynamics, it can be reconciled with ETH [40] by ensuring that $\beta = 0$ in eq 1. It can be reconciled with ETH by ensuring that the RHS of eqn 1 is independent of β , i.e., an infinite temperature ensemble [40]. In other words, the nonequilibrium steady state of the system tends to an infinite temperature, maximum entropy density matrix.

However, drive parameters like amplitude, frequency, and duty-cycle strongly affect the structure of the Floquet modes $|\phi\rangle$. Thus, they can be engineered to prevent the kind of full mixing that would lead to infinite temperatures, manifesting suppression of thermalization dynamically. Thus, this type

of *Floquet Engineering* can produce *Dynamical Many Body Localization* (DMBL), where the system fails to reach thermal equilibrium and remains localized, possibly near its initial state, even at large times. This paradigm seems similar to standard Many-Body Localization[41, 42], where disorder, locality, and integrability can cause athermality via breakdown in the Srednicki ansatz. However, DMBL is a ~~purely dynamical phenomenon~~ stems from periodic driving, and thus can occur regardless of disorder, locality of observables, or system integrability, all of which have been studied for MBL onset [43–45].

Integrable Many Body systems do not exhibit thermalization. When subjected to time-periodic drives, Floquet engineering allows for the introduction of additional approximate conserved quantities that dynamically suppress the evolution of certain observables by hysteresis. This type of *freezing* of response has been shown in integrable systems [6]. A paradigmatic example is the driven Transverse Field Ising model (TFIM) in one dimension [46]. The Hamiltonian is given by

$$\hat{H}(t) = \hat{H}_0 + h_z(t) \hat{H}_1, \quad (6)$$

$$\hat{H}_0 = -\frac{1}{2} \sum_{i=1}^N \sigma_i^x \sigma_{i+1}^x, \quad (7)$$

$$\hat{H}_1 = -\frac{1}{2} \sum_{i=1}^N \sigma_i^z. \quad (8)$$

Here, the undriven Hamiltonian \hat{H}_0 consists of nearest-neighbour interactions between N number of spin-1/2 particles on a one-dimensional spin network. The transverse field is denoted by \hat{H}_1 , and is being varied by a time-periodic and harmonic signal $h_z(t) = h_0 + h \cos \omega t$, yielding a time period $T = 2\pi/\omega$ with amplitude h , drive frequency ω , and d.c. field h_0 . This Hamiltonian can be readily transformed into a spinless pseudo-fermionic system via the Jordan-Wigner transformation [4]. When written in momentum space spanned by spinors $\psi_k = (c_{-k}, c_k^\dagger)^T$ of fermions at momentum k created (annihilated) by operators c_k^\dagger (c_k), the effective Hamiltonian

$$H(t) = \sum_{(k,-k)-\text{pairs}} \psi_k^\dagger \left[\left(f_k - h_z(t) \right) \tau_z + \tau_x \Delta_k \right] \psi_k, \quad (9)$$

where $f_k = \cos k$, $\Delta_k = \sin k$, τ_{xyz} are the three Pauli Matrices, and the sum is over distinct $(k, -k)$ Cooper Pairs. We can transform our system to a frame that rotates with the time-varying symmetry-breaking field. This is achieved by the means of the unitary transfor-

mation operator

$$U(t) = \prod_k U_k(t) \quad (10)$$

$$U_k(t) = \exp \left\{ \left[\frac{i\hbar}{\omega} \sin \omega t \right] \tau_z \right\}.$$

The resulting transformed Hamiltonian $H'(t) = U^\dagger(t) H(t) U(t) - iU^\dagger(t) \partial_t U(t)$ simplifies to

$$H'(t) = \sum_{(k,-k)-\text{pairs}} \psi_k^\dagger \left[\tau_z f_k + \tau_x \cos(\eta \sin \omega t) + \tau_y \sin(\eta \sin \omega t) \right] \psi_k, \quad (11)$$

where we defined $\eta = 2\hbar/\omega$. Using the Jacobi-Anger formula [47]

$$e^{i\eta \sin \omega t} = \sum_{n=-\infty}^{\infty} J_n(\eta) e^{in\omega t}, \quad (12)$$

where $J_n(\eta)$ are Bessel Functions, the transformed Hamiltonian simplifies to

$$H'(t) = \sum_{(k,-k)-\text{pairs}} \psi_k^\dagger \left\{ \tau_z f_k + 2\tau_x \Delta_k \sum_{n \geq 0} J_{2n}(\eta) \cos(2n\omega t) - 2\tau_y \Delta_k \sum_{n \geq 0} J_{2n+1}(\eta) \sin[(2n+1)\omega t] \right\} \psi_k. \quad (13)$$

In the frequency regime $\omega \gg f_k$, the long-time average $H^{RWA} \equiv \lim_{n \rightarrow \infty} \frac{1}{nT} \int_0^{nT} dt H'(t)$ can serve as a suitable approximation for $H'(t)$. This approximation, known as the *Rotated Wave Approximation* (RWA), eliminates the oscillating modes and results in an effective Hamiltonian that is independent of time,

$$H^{RWA} = \sum_{(k,-k)-\text{pairs}} \psi_k^\dagger \left[f_k \tau_z + 2J_0(\eta) \Delta_k \tau_x \right] \psi_k. \quad (14)$$

It is evident that by manipulating the drive parameters, specifically the amplitude denoted by h and the frequency denoted by ω , in a manner such that η is positioned on a root of $J_0(\eta)$, the fermion number can be conserved to a significant extent at this particular resonance. Consequently, it is feasible to exercise direct control over H^{RWA} , resulting in a comprehensive suppression of the dynamics of otherwise responsive observables.

This phenomenon is highly general in nature, and can be readily adapted to non-integrable systems. In

such cases, freezing has the additional effect of inducing DMBL, suppressing thermalization to infinite temperatures. Numerical quantification of localization of a specific (quasi) stationary state in a physically significant representation can be achieved through the computation of the *Inverse Participation Ratio* (IPR). The IPR is generally defined as the formal sum over the square of the local density in a physically meaningful space. [48–51] In the single particle case, the IPR, for a state $|\psi\rangle$ can be written as

$$\phi_{IPR} \equiv \int d\mathbf{x} |\langle \mathbf{x} | \psi \rangle|^4.$$

267 This definition can be generalized applied to obtain
268 the IPR of a state $|\phi\rangle$ in a representation given by any
269 complete orthonormal single particle basis $|m\rangle$ as

$$\phi_{IPR} \equiv \sum_m |\langle m | \psi \rangle|^4. \quad (15)$$

270 The smallest value of the IPR corresponds to a fully
271 de-localized state, $\psi(x) = 1/\sqrt{N}$ for a system of size
272 N [51, 52]. Values of the IPR close to unity correspond
273 to localized states [53]. For a periodically driven sys-
274 tem, we look at the IPR of the quasi-stationary Floquet
275 modes at $t = T$, where $t = 2\pi/\omega$ for drive frequency ω .
276 In the TFIM model, equation 14 indicates that, at reso-
277 nance, when $J_0(\eta) = 0$, the Floquet modes are approx-
278 imately given by the fermionic Fock states, which have
279 a trivially unit IPR in the representation of the eigen-
280 modes of the transverse field \hat{H}_1 in equation 6. Here, a
281 particular Floquet mode can be decomposed into a di-
282 rect product of cooper-pair states as $|\phi\rangle = \prod_{k,-k} |\phi_k^n\rangle$.
283 In the RWA limit and at resonance, $|\phi_k^n\rangle$ has values of
284 $|0\rangle, |k, -k\rangle$ for two values of $n = 0, 1$ respectively. We
285 define the reduced IPR of $|\phi_k^n\rangle \forall k$ to be

$$\phi_{IPR}^{(n)}(k) = |\langle 0 | \phi_k^n \rangle|^4 + |\langle +k, -k | \phi_k^n \rangle|^4, \quad (16)$$

286 where $n = 0, 1$. In the RWA limit and at resonance ,
287 this quantity is unity, indicating very low participation
288 and the onset of freezing. Figure 1 shows results from
289 numerically simulating the TFIM dynamics. The re-
290 duced IPR for a particular Floquet mode recovered by
291 simulating the exact Schrödinger dynamics over a sin-
292 gle time period of the drive, and plotted as a function
293 of momentum k for different η 's. At resonance, when
294 η lies at the root of the Bessel function $J_0(\eta)$, the IPR
295 is exactly nearly unity for all momenta. Outside this
296 resonance, the IPR is unity only for some momenta
297 because the effective Hamiltonian is perfect diagonal
298 at $k \in \{-\pi, 0, \pi\}$ as can be seen in the cross-sectional
299 plots of figure 1. As we move away from the resonance
300 point, IPR reduces from unity. However, as the TFIM
301 is an integrable spin model, the IPR never drops to a
302 value that is small enough to indicate thermalization.
303

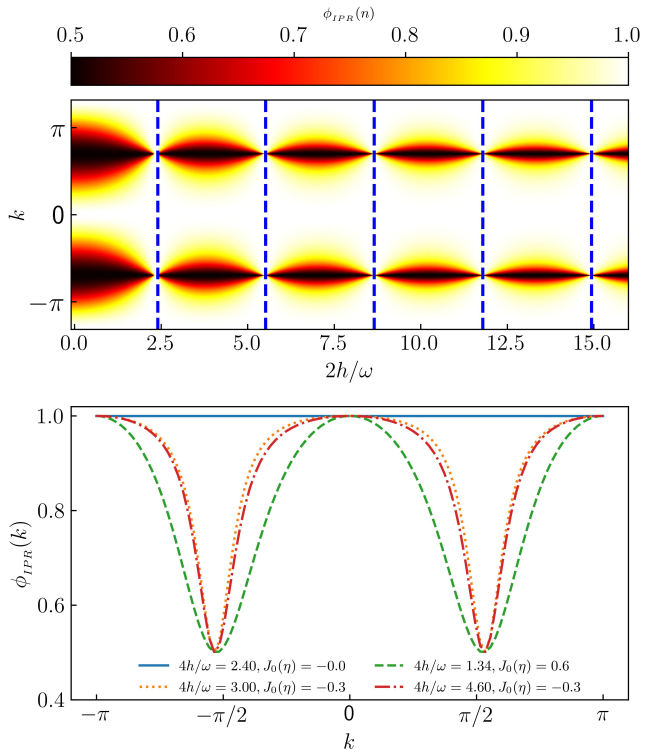


FIG. 1. Reduced IPR (defined in equation 16) for one of the two Floquet modes obtained from the exact dynamics of the TFIM for size $N = 100$ and $\omega = 90$ for the entire Brillouin zone (top panel, ordinate) and a few drive amplitudes (top panel, abscissa). The dashed lines (top panel) indicate the roots of $J_0(\eta)$. The bottom panel shows cross-sections for four different chosen amplitudes.

304 At low frequencies, RWA fails due to the unavailability
305 of zero off-diagonal terms in the effective transformed
306 Hamiltonian, as well as the absence of integrability
307 breaking terms to counteract the off diagonal terms.

308 Consequently, the IPR remains quite high (~ 0.5) even
309 at the resonance point as can be seen figure 1. At low
310 frequency, this is valid for all momentum and param-
311 ter η , see figure 2.

312 Because the dependence of observable expectations
313 on the eigenstates is always fairly strong for inte-
314 grable systems like the TFIM, such systems will never
315 exhibit any kind of thermal behaviour unless integra-
316 bility breaking terms (such as strong disorder) are in-
317 cluded [6]. As a result, it is not physically meaningful
318 to refer to the unit IPR region as "Many Body Localiza-
319 tion", because the parameter space lacks a thermal-
320 ized region to contrast with this state. The type of Flo-
321 quet Engineering described above, on the other hand,
322 can be easily applied to a broad class of nonintegrable
323 systems where FETH is expected to hold in certain re-
324 gions. Long-range spin systems, in particular, where

See an-
notation.

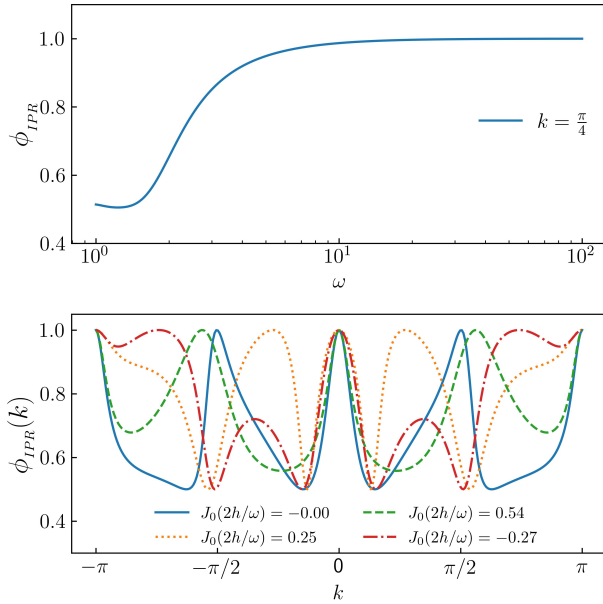


FIG. 2. Reduced IPR obtained by adiabatically increasing ω (top panel abscissa) for one the floquet mode obtained from equation 16 at the root of $J_0(\eta)$ for $N = 500$. IPR is ~ 0.5 (localized yet not fully freezing) upto $\omega \sim 2$, after that, smoothly increased to unity (fully localized and freezing) at higher $\omega \geq 10$ (top panel, ordinate). At bottom panel cross-sections for four chosen amplitudes at $\omega = 2$ are plotted for a brillouin zone (abscissa) with corresponding reduced IPRs (ordinate).

the exchange energies between far-off spins are taken into account in the model Hamiltonian, are good candidates because they are known to thermalize when driven with low frequencies [54].

II. LONG RANGE INTERACTIONS: THE LIPKIN MESHKOV GLICK MODEL:

The periodically driven Curie-Weiss Lipkin Meshkov Glick (LMG) model [20, 55] for N long-range spins is described by the Hamiltonian

$$\hat{H}(t) = \hat{H}_0 + [h \cos(\omega t) + h_0] \hat{H}_1. \quad (17)$$

Here, the undriven part \hat{H}_0 and the driven part \hat{H}_1 are, respectively,

$$\hat{H}_0 = \frac{2}{N-1} \sum_{ij} \hat{\sigma}_i^z \hat{\sigma}_j^z,$$

$$\hat{H}_1 = \sum_{i=1}^N \hat{\sigma}_i^x.$$

The Kac-norm of $2/(N-1)$ arises from the choice to maintain the extensivity of the interaction energy. The Hamiltonian in equation 17 commutes with $P_{ij} \equiv \frac{1}{2} (1 + \vec{\sigma}_i \cdot \vec{\sigma}_j)$. In addition, it also commutes with the total angular momentum $S^2 = |\vec{S}|^2$, where $\vec{S} = S^x \hat{x} + S^y \hat{y} + S^z \hat{z} \equiv \frac{1}{2} \sum_i \vec{\sigma}_i$. We now choose to populate the system in a state with $S^2 = \frac{N}{2} \left(\frac{N}{2} + 1 \right)$. In that case, the dynamics remains invariant in the $N+1$ -dimensional space spanned by the common eigenstates of P_{ij} , $|S|^2$ and S_z ; the so-called *Totally Symmetric Subspace*, or TSS [56]. Let the eigenvalues of S^z in the TSS be s_n , and the eigenvectors be $|s_n\rangle$. Here, $s_n = -\frac{1}{2} + \frac{n}{N}$ and the index $n = 0(1)N$ has $N+1$ values. The dynamics is restricted to this invariant subspace, wherein the matrix elements of the Hamiltonian are given by

$$\begin{aligned} \langle s_i | \hat{H}_0 | s_j \rangle &= -\frac{4}{N-1} s_i^2 \delta_{ij}, \\ \langle s_i | \hat{H}_1 | s_j \rangle &= \left[\sqrt{\frac{N}{2} \left(\frac{N}{2} + 1 \right) - N s_i (N s_{i+1})} \delta_{i+1,j} \right. \\ &\quad \left. + \sqrt{\frac{N}{2} \left(\frac{N}{2} + 1 \right) - N s_i (N s_{i-1})} \delta_{i-1,j} \right]. \end{aligned} \quad (19)$$

These allow for a numerical representation of the Hamiltonian in the TSS.

Next, we transform the Hamiltonian to the rotated frame given by the operator

$$\hat{U}(t) = \exp \left[i \frac{h}{\omega} \sin(\omega t) \hat{H}_1 \right]. \quad (20)$$

This is analogous to the rotation performed for the TFIM in eqns 10 and 11. Defining $\tau = \frac{h}{\omega} \sin \omega t$, we use the fact that $\hat{H}_1 = 2S^x$, as well as the following identity obtained by using the Baker-Campbell-Hausdorff formula,

$$e^{i2\tau \hat{S}^x} \hat{S}^z e^{-i2\tau \hat{S}^x} = \hat{S}^z \cos(2\tau) + \hat{S}^y \sin(2\tau), \quad (21)$$

to simplify the transformed Hamiltonian $\tilde{H}(t) = \hat{U}^\dagger(t) \hat{H}(t) \hat{U}(t) - \hat{U}^\dagger(t) \partial_t \hat{U}(t)$, yielding

$$\begin{aligned} \tilde{H}(t) &= -\frac{1}{N-1} \left[(S^z)^2 (1 + \cos 4\tau) + (S^y)^2 (1 - \cos 4\tau) \right. \\ &\quad \left. + \{S^y, S^z\} \sin 4\tau \right] - 2h_0 S^x. \end{aligned} \quad (22)$$

Next, we define $\eta \equiv 4h/\omega$ and use the Jacobi-Anger formula in eqn 12 to expand $\tilde{H}(t)$. This yields

$$\tilde{H}(t) = -\frac{\hat{S}^2}{N-1} + \frac{(\hat{S}^x)^2}{N-1} - 2h_0\hat{S}^x - \frac{J_0(\eta)}{N-1} \left[(\hat{S}^z)^2 - (\hat{S}^y)^2 \right] - \frac{2}{N-1} \left[(\hat{S}^z)^2 - (\hat{S}^y)^2 \right] \sum_{k=1}^{\infty} J_{2k}(\eta) \cos(2k\omega t) - \frac{2}{N-1} \{ \hat{S}^y, \hat{S}^z \} \sum_{k=1}^{\infty} J_{2k-1}(\eta) \sin[(2k-1)\omega t]. \quad (23)$$

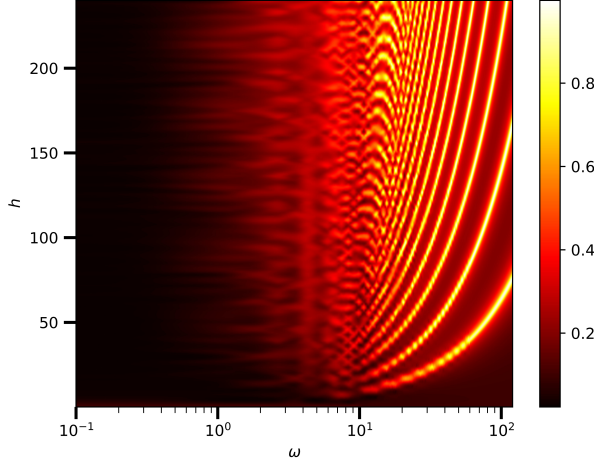


FIG. 3. Plot of the numerically averaged IPR (IPR computed using eqn 26) in the TSS plotted in the $h - \omega$ plane for $N = 100$ spins. In order to display the thermalized region more clearly, ω is plotted on a logarithmic scale on the abscissa. Note that, since the IPR is clearly non-negative, an average IPR of zero means that all Floquet states have zero IPR. Furthermore, the boundedness of IPR in $\phi_{IPR}(n) \leq 1$ ensures that if the average IPR is unity, then all Floquet states have unit IPR.

If ω is large enough to smooth out the harmonic components, we obtain the RWA,

$$\tilde{H}(t) \approx \tilde{H}_{\text{RWA}} \equiv -\frac{\hat{S}^2}{N-1} + \frac{(\hat{S}^x)^2}{N-1} - 2h_0\hat{S}^x - \frac{J_0(\eta)}{N-1} \left[(\hat{S}^z)^2 - (\hat{S}^y)^2 \right]. \quad (24)$$

If the drive amplitude h is adjusted such that η lies at a root of $J_0(\eta)$ (the localization point), the RWA Hamiltonian is diagonal in the representation of the simultaneous eigenstates of transverse field \hat{S}^x , and S^2 , yielding an IPR of unity in that representation, similar to the TFIM in the previous section. Note however, that if the DC transverse field h_0 is set to 0, then, at the localization point, the RWA Hamiltonian $\tilde{H}_{\text{RWA}} \sim (\hat{S}^x)^2$ in the TSS. The eigenvalues are two-fold degenerate. This produces infinitely many (Floquet) eigenmodes in the degenerate subspace whose IPRs may not always

be unity in the S^x representation. The removal of this degeneracy necessitates the inclusion of the d.c. field h_0 . However, note that rational values of h_0 may add accidental degeneracies in \tilde{H}_{RWA} . To see this, note that, at a localization point, the eigenvalues of \tilde{H}_{RWA} in the TSS are given by

$$\text{Eigs}[\tilde{H}_{\text{RWA}}] = \frac{\left(\frac{N}{2} - m\right)^2}{N-1} - 2h_0 \left(\frac{N}{2} - m\right), \quad (25)$$

where the half-integer $-N/2 \leq m \leq N/2$ is the eigenvalue corresponding to a particular eigenstate $|m\rangle$ of the symmetry-breaking field \hat{S}^x . In order to ensure that no additional degeneracies occur, we have to set h_0 in such a way that no two energies accidentally coincide. If $N \gg 1$ (substantially large), then this condition can be readily met by assuring that $(1 - 2h_0)^{-1}$ is never an integer that is divisible by N . To ensure this in our numerical simulations, we have kept h_0 at a small irrational value. The localization of the Floquet states at resonance is supported by exact numerical results, as can be seen in the phase diagram fig 3. Here, we have plotted the arithmetic mean over all Floquet states of the IPR in the TSS for each point in the $h - \omega$ plane for $N = 100$ spins. The IPR in S^x representation is

$$\phi_{IPR}(n) = \sum_m |\langle m | \phi^n \rangle|^4. \quad (26)$$

As can be readily seen in the figure, the IPR is essentially zero when $\omega \lesssim 1$. There is considerable structure in the phase diagram for larger drive frequencies, and along the lines given by the roots of $J_0(\eta)$, the IPR is essentially unity, in agreement with eqn. 24.

In figure 4, we show plots of the IPR of the Floquet modes $|\phi^n\rangle$ for $S^2 = (N/2)(N/2+1)$. These plots were obtained numerically by diagonalizing the propagator $U(t)$ at $t = T$, where $U(t)$ is defined in eqn 5. This propagator was obtained from simulations of the exact quantum dynamics using QuTiP, the Quantum Toolbox in Python [57]. We kept the frequency at a fairly large value $\omega = 90$ where we expect that RWA would be valid, and $N = \mathcal{O}(10^2)$. The density plot in the upper panel of fig 4 depicts the IPR of the Floquet states; the abscissa $\eta = 4h/\omega$ and the ordinate is $n/(2N+1)$, where $n \leq 2N$ is a non-negative integer

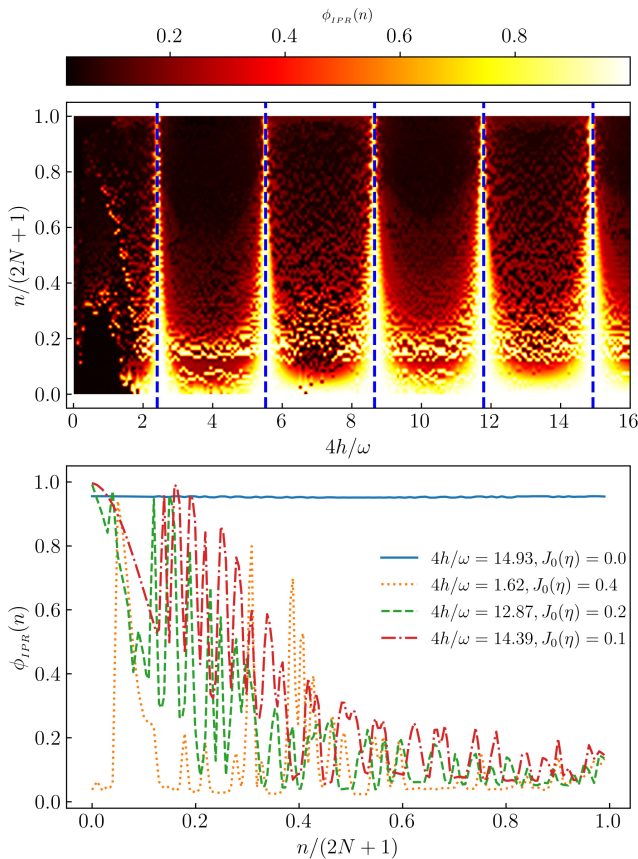


FIG. 4. IPR density plot for all possible Floquet modes (top panel ordinate) for different values of $\eta = 4h/\omega$ (top panel abscissa), deduced from equation 26 for exact LMG Hamiltonian for $N = 50$. Blue dashed lines are roots of $J_0(\eta)$. At bottom panel cross-section of IPR (ordinate)for four different η 's plotted for all possible floquet modes(bottom panel, abscissa) at $\omega = 90$. IPR founds to be \sim unity for all Floquet modes at roots of J_0 .

400 that indexes the Floquet states in increasing order of
 401 m . The dashed vertical lines correspond to the roots
 402 of $J_0(\eta)$. Comparing with the IPR of the TFIM in fig 1,
 403 we can see a very similar patterns in the immediate
 404 neighbourhood of the roots. Evidently, the IPR ap-
 405 proaches a value of one for sufficiently large values of
 406 the roots, strongly suggesting full DMBL. Deviations
 407 occur at the smallest root of $J_0(\eta)$ (around $\eta = 2.405$).
 408 due to the contributions from higher order terms in
 409 eq 23. Thus, a higher root is favored for DMBL.

410 The bottom panel of fig 4 contains cross sections
 411 of the full IPR plot for selected values of η as indi-
 412 cated in the legend. When the drive amplitude h is
 413 adjusted such that η is close to a root of $J_0(\eta)$, the Flo-
 414 quet States are mixed, but not entirely thermal, since
 415 the IPR does not fall to $\mathcal{O}(N^{-1})$, indicating that local-
 416 ization persists to some extent. However, the further
 417 we are from the roots, the closer the IPR gets to one
 418 predicted by thermalization.

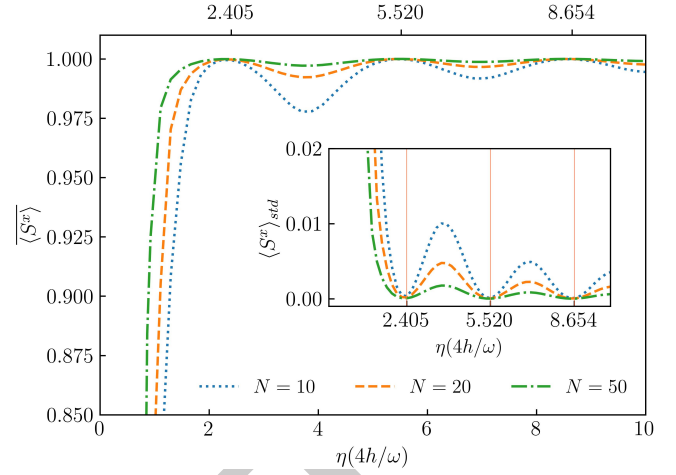


FIG. 5. Temporal average of $\langle \hat{S}^x \rangle$ (ordinate) for different η 's (abscissa) is plotted for $\sim 200T$ at higher ω for different $N=10, 20, 50$. $\langle \hat{S}^x \rangle$ is found to be unity at roots of $J_0(\eta)$. At points away from resonance points, $\langle \hat{S}^x \rangle$ falls below unity. The corresponding standard deviation $\langle \hat{S}^x \rangle_{std}$ supports the variation of $\langle \hat{S}^x \rangle$ (inset fig.). $\langle \hat{S}^x \rangle_{std}$ is ~ 0 describing a full freezing of the system at roots of $J_0(\eta)$ (red vertical solid lines).

419 Figure 5 shows plots of the long-time average (from
 420 $t = 0 - 200T$) of the field amplitude $\langle \hat{S}^x \rangle$ as a function
 421 of η . The system is started from the fully polarized
 422 state $s_n = N/2$ in the TSS and the dynamics simulated.
 423 The average is plotted for different values of ampli-
 424 tude h , keeping the frequency fixed at a high value of
 425 $\omega = 90$. It is clearly very close to unity at roots of $J_0(\eta)$
 426 and falls at points away from it, indicating that S^x is
 427 approximately conserved at the localization points.

428 Small deviations do occur due to the role of higher
 429 order terms in the rotated Hamiltonian in eq 22. This
 430 can be demonstrated quantitatively by comparing the
 431 IPR obtained from the exact dynamics simulation with
 432 that obtained from the dynamics of $\tilde{H}(t)$ in eq. 22 after
 433 truncating the series at orders $k \geq 1$. This compari-
 434 son can be seen in fig 6. The IPR plots from the ex-
 435 act dynamics indicate that the first localization point,
 436 represented by the lowest root of $J_0(\eta)$, does not show
 437 complete DMBL. However, DMBL is particularly con-
 438 spicuous at large roots. The IPRs of the Floquet states
 439 obtained from the RWA dynamics exhibit large devia-
 440 tions from unity when away from the localization point
 441 as evidenced by the green and red curves in the mid-
 442 dle panel of fig 6. However, complete localization is
 443 seen in the RWA dynamics at any localization point, in
 444 contrast to the exact case in the top panel. Thus, it
 445 is necessary to incorporate higher-order corrections
 446 into the Rotating Wave Approximation (RWA) at lower

452 III. PERSISTENCE OF DMBL IN THE CONTINUUM
453 LIMIT

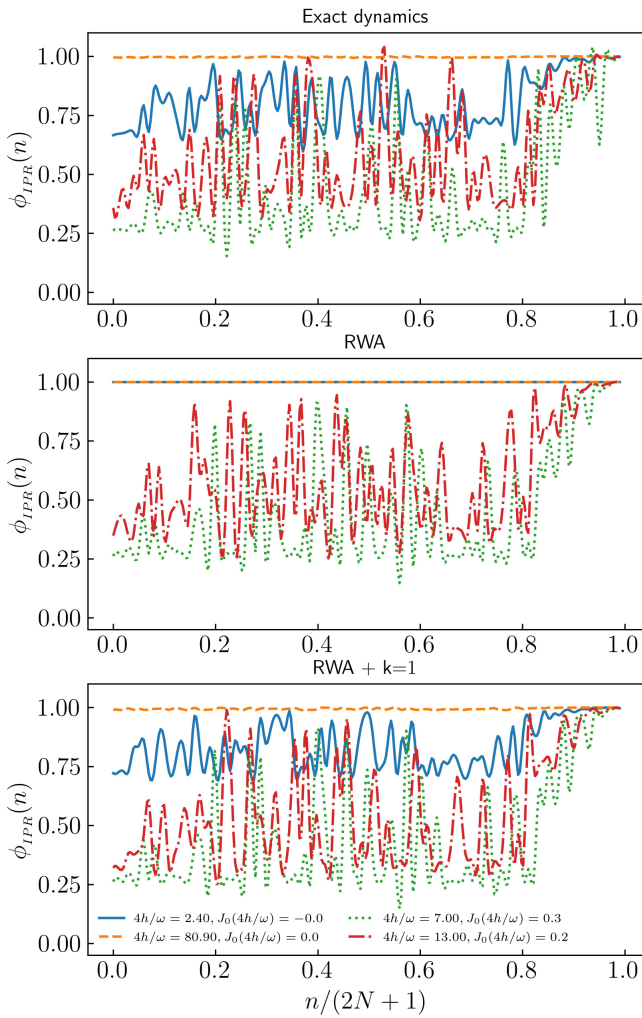


FIG. 6. The comparison between IPR for exact dynamics and RWA with corresponding correction orders. IPR is calculated for four different η 's and corresponding $J_0(\eta)$ values for colors, Blue : $\eta = 2.40, J_0(\eta) = 0.0$, dashed orange: $\eta = 80.9, J_0(\eta) = 0.0$, Green: $\eta = 7.0, J_0(\eta) = 0.3$, Red: $\eta = 13, J_0(\eta) = 0.2$. At low root of $J_0(\eta)$ IPR is not unity (Blue curve) where at higher root (orange dashed) it is unity while at points away from roots IPR are less than unity in the exact (top panel) plot. RWA does not matches with the exact plot. At all roots of $J_0(\eta)$ IPR is unity(middle panel). RWA with additional higher order terms exhibit similar system pattern(Bottom panel) with exact dynamics.

448 localization points. The application of the first-order
449 correction to RWA in the lower panel of fig 6 results in
450 a curve structure that is closer to that from the exact
451 dynamics.

454 In the continuum limit, where $N \rightarrow \infty$, the disparity
455 between neighboring values of s_i in equation 19 can
456 be disregarded, and s_i can be mapped to a continuum
457 $q \in [-1/2, 1/2]$ [56]. We define the Hamiltonian per
458 particle $h(t) \equiv \frac{H(t)}{N}$, and a canonically conjugate co-
459 ordinate $Np \equiv \left\langle -i \frac{\partial}{\partial q} \right\rangle$. Then, in this limit, the dynam-
460 ics can be approximated by that of a classical Hamil-
461 tonian [58]

$$h(t) = -2q^2 - [h \cos \omega t + h_0] \sqrt{1 - 4q^2} \cos p, \quad (27)$$

which yields the dynamical system

$$\begin{aligned} \frac{dq}{dt} &= \frac{\partial h}{\partial p} = h(t) \sqrt{1 - 4q^2} \sin p \\ \frac{dp}{dt} &= -\frac{\partial h}{\partial q} = 4q \left[1 - \frac{h(t) \cos p}{\sqrt{1 - 4q^2}} \right], \end{aligned} \quad (28)$$

462 where $h(t) = [h \cos \omega t + h_0]$. We have profiled simula-
463 tions of the ensuing dynamics with the *Poincaré sur-*
464 *face of section* (PSOS) of the full dynamics. Here, the
465 (q, p) -phase space is strobed at $t = nT$, and plotted
466 for a large number of initial conditions. The results
467 are shown in the upper panels of fig 7 for a small value
468 of $\omega = 2.0$ (left panel) and a large value $\omega = 90$ (right
469 panel). In both cases, the value of h is chosen such
470 that η lies on the first root of $J_0(\eta)$. The onset of chaos
471 for small drive frequency indicates thermal behaviour
472 for typical initial conditions, with small islands of reg-
473 ularity for others. This is consistent with similar re-
474 sults for small frequencies reported in [54, 59]. How-
475 ever, at high frequency, the regular islands distinctly
476 dominate over the chaos. The trajectories indicate
477 that the conservation of $\langle S^x \rangle \approx \sqrt{1 - 4q^2} \cos p$ [56]
478 at high ω persists in the thermodynamic limit. That
479 this is a signature of the underlying quantum dynam-
480 ics can be readily seen in the quantum phase space
481 representation of the Floquet Eigenstates for a large
482 but finite N . These are shown in the correspondingly
483 lower panels of fig 7. Here, we have plotted the Spec-
484 tral Average of the Husimi Q-functions of the acquired
485 Floquet States in the TSS. Specifically, for a coher-
486 ent state $|q, p\rangle$, the corresponding Spectral-Averaged
487 Husimi distribution [60] is obtained by

$$H(q, p) \equiv \frac{1}{(2N+1)\pi} \sum_n \langle q, p | \phi^n \rangle \langle \phi^n | q, p \rangle. \quad (29)$$

488 The quantum phase space retains signatures of the
489 classical phase space dynamics when $N = 100$, indi-
490 cating the onset of the persistence of S^x conservation
491 that arises from the resonance condition at high fre-
492 quencies.

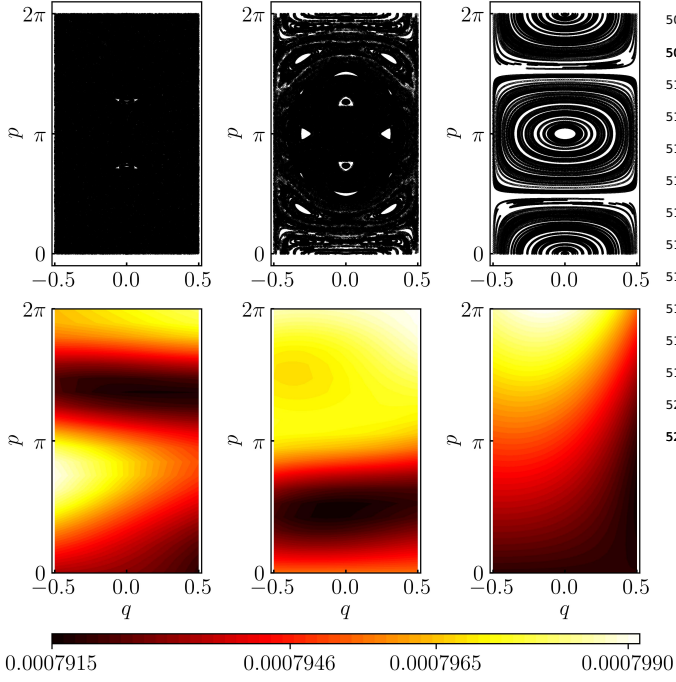


FIG. 7. Phase-space distributions at $\omega = 1.0$ (left panels), $\omega = 2.5$ (middle panels) and $\omega = 90.0$ (right panels) for 100 initial conditions. The drive amplitude h is always adjusted such that $\eta = 4h/\omega$ lies on the smallest root of $J_0(\eta)$, i.e. $\eta = 2.4048\dots$. At small $\omega = 1.0$, the classical PSOS, obtained from simulating the dynamics in eqns 28 (top left panel), shows chaotic behaviour, and at $\omega = 2.5$, regular regions start to appear. At higher $\omega = 90.0$, the dominance of regular dynamics can be readily seen (top right panel). The bottom panels plot the corresponding Spectral-Averaged Husimi-Q function, obtained from the Floquet modes $|\phi^n\rangle$ using eqn. 29, and setting $N = 100$. The $\omega = 1.0$ case (bottom left panel) has a dispersed distribution in colour. This is consistent with the chaotic behaviour seen in the continuum limit. At $\omega = 2.5$ (bottom middle panel), there is a partial regular pattern observed together with a dispersed pattern. In the $\omega = 90$ -case (bottom right panel), the distribution has distinct colour contrasts, which is consistent with the regular dynamics pattern seen in the continuum limit.

494 IV. PHASE CROSSOVER FROM THERMAL TO DMBL

495 The analysis of the periodically driven LMG model
496 reveals two distinct scenarios at low and high external
497 drive frequencies. In the former case, thermalization
498 in accordance with FETH is seen, whereas in the latter
499 case, DMBL is induced. As a result, we hypothesize
500 that a macroscopic change in phase occurs due to the
501 influence of frequency.

502 To demonstrate this, we investigate the IPR of the
503 Floquet mode with smallest quasienergy for numer-
504 ous frequencies and system sizes, along with the as-
505 sociated drive amplitude h keeping the system at a lo-
506 calization point. The results are shown in fig 8. In the

507 low-frequency range $\omega \in [1.0, 9.0]$, the IPR exhibits val-
508 ues well below unity. Moreover, the IPR gradually di-
510 minishes with increasing system size, following a sys-
511 tem size inverse proportional trend, which confirms
512 the participation distribution (as shown in the bottom
513 panel). As the limit $N \rightarrow \infty$, the inverse participation
514 ratio (IPR) tends towards zero, indicating a fully de-
515 localized state. The plots reveal a gradual increase
516 in the unity of IPR over a certain frequency range,
517 specifically at $\omega \approx 5$. In addition, the rise does not
518 cross with those for different values of N , suggesting
519 the onset of a phase crossover [42, 61]. As the size of
520 the system increases, the crossover region becomes
521 smoother, rather than sharper.

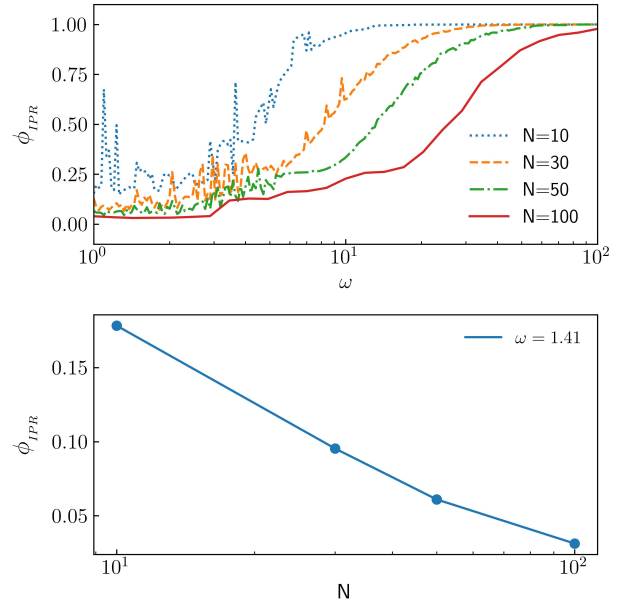


FIG. 8. IPR is plotted (top panel, ordinate) for a range of $\omega \in [1, 100]$ (top panel, abscissa) for four different $N = 10, 30, 50, 100$ at root of $J_0(\eta)$. At small ω upto $\omega \sim 10$ IPR founds to be very small and rises slowly upto unity (fully localized) at higher frequencies. At bottom panel IPR (ordinate) is plotted for different $N = 10, 30, 50, 100$ (bottom panel, abscissa) for a random small $\omega \sim 1$ at root of $J_0(\eta)$ from the values from top panel. IPR falls as inversely proportional to N , indicating an approach to a fully distributed (thermal) state. The smooth rise in IPR defines a phase crossover (top panel) between a fully thermal phase to a fully localized phase.

524 We can also look at this crossover more clearly in
525 the plots of the heating rate of the system, defined
526 simply by the expectation value of the Hamiltonian,
527 $\langle \hat{H}(t) \rangle$. We have carried out the numerical evaluation
528 from the simulated dynamics over $t = 500T$. When the
529 system is adequately described by FETH, the temporal
530 fluctuations in the heating-rate Hamiltonian, defined

How to identify the crossover frequency in the semiclassical? In fig. 7, it looks like conserved quantities appear at middle panel, $\omega = 2.5$, same place where IPR starts to rise in fig. 8. Is that good enough?

We're working on doing this thing outside the J_0 root.

532 by $\langle H \rangle_{std}^2 \equiv \overline{\langle \hat{H} \rangle^2} - \overline{\langle \hat{H} \rangle}^2$ (see eqn 3), are minimal in
 533 the thermodynamic limit, as the spread of states leads
 534 to a limited standard deviation[62]. Conversely, the
 535 onset of athermalism is indicated by nonzero fluctua-
 536 tions in time. If we set the initial state to the fully po-
 537 larized state in the TSS (given by $|s_N\rangle$), then the onset
 538 of freezing, together with DMBL, will result in nearly
 539 infinite hysteresis in the ensuing dynamics, causing
 540 $|\psi\rangle(t) \approx |s_N\rangle \forall t$. From eqn. 17, we can clearly see
 541 that this will lead to a linearly rising dependence on
 542 ω in $\langle H \rangle_{std}$ as long as we stick to a **localization point**
 543 given by a fixed h/ω [63]. All these observations are
 544 corroborated by the heating rate plots in figure 9.

There is
a new
footnote.

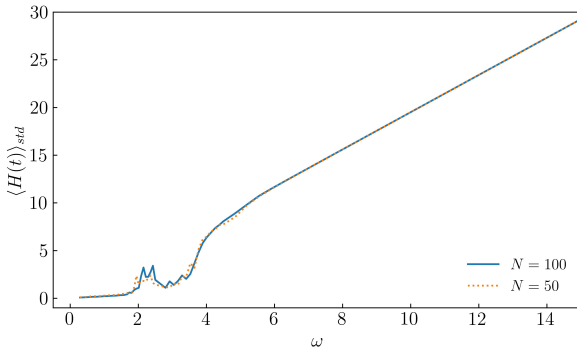


FIG. 9. The standard deviation of the heating rate, denoted by $\langle H \rangle_{std}$, calculated over a span of $t = 500T$ for two system sizes. Here, h is varied to keep $\eta = 4h/\omega$ at the first root of $J_0(\eta)$. A nonsingular rise has been identified at $\omega \approx 4.0$. $\langle H \rangle_{std}$ exhibits a diminutive magnitude below that value of ω , while a linear rise is observed at higher frequencies, consistent with freezing. A vanishingly small standard deviation for $\omega \ll 4.0$ indicates the presence of a thermal region, whereas a larger finite standard deviation suggests the existence of athermal behaviour. The small peaks observed at $\omega \in [2, 4]$ are finite-size effects that disappear in the thermodynamic limit.

546

547

548

V. CONCLUSION AND OUTLOOK

549 We have delved into the onset of freezing and
 550 phase cross-over in 1D spin systems driven by a time-
 551 periodic transverse field, contrasting the responses
 552 in the Transverse Field Ising Model (TFIM) with that
 553 of the long-range Lipkin-Meshkov-Glick Model (LMG).
 554 The parametrization of DMBL is based on the Inverse
 555 Participation Ratio (IPR) of the Floquet eigenstates.
 556 Our investigations compared the IPRs from both mod-
 557 els numerically, and found the emergence of thermal
 558 behavior at low frequencies and freezing at high fre-

559 quencies for the LMG model, the latter a direct conse-
 560 quence of the appearance of additional approximately
 561 conserved quantities.

562 Long-range spins exhibit strong localization in spin-
 563 coordinate space for the LMG model when the drive
 564 frequency is $\omega \gg J$, where J represents the spin ex-
 565 change energy. The localization of the LMG model
 566 occurs at specific resonance points of the drive fre-
 567 quency ω and amplitude h , at $J_0(4h/\omega) = 0$, $\omega \gg J$.
 568 This is apparently similar to the phenomenon of Dy-
 569 namical Freezing (DMF) in the Transverse Field Ising
 570 Model (TFIM), where comparable localization at res-
 571 onance points, determined by the roots of $J_0(2h/\omega)$,
 572 occurs due to the onset of an additional approximate
 573 conservation in the transverse field itself. However,
 574 a key difference is the thermal behaviour of the LMG
 575 model at low frequencies. Plots of the IPR for a range
 576 of frequencies along the resonance manifold exhibits
 577 a smooth increase in IPR yielding a quantum phase-
 578 crossover from a thermal phase governed by the Flo-
 579 quet Eigenstate Thermalization Hypothesis (FETH) to
 580 a Dynamically Many-Body localized phase (DMBL).
 581 This crossover is absent in the TFIM, as can be readily
 582 seen in the significant magnitude of the inverse par-
 583 ticipation ratio (IPR) even at low frequencies. Thus,
 584 the suppression of thermalization through Dynamical
 585 Many Body Localization in long-range systems can be
 586 controlled via Floquet engineering, even in clean sys-
 587 tems without any disorder. Thus, periodically driven
 588 long-range spin systems are an excellent tool for in-
 589 vestigating disorder-free Many Body Localization, as
 590 can be readily seen via the IPR of its Floquet modes.

591 There are several unexplored indicators of DMBL,
 592 such as entanglement entropy and level statistics [10],
 593 which we defer to future studies. In addition,
 594 Halpern in 2019 proposed a quantum engine based
 595 on MBL[11] which works between strong localized
 596 and thermal phases of the system. In our proposed
 597 LMG model, tuning the system parameters by bring-
 598 ing them to the resonance points, then adiabatically
 599 cycling the frequency from the thermal region to the
 600 DMBL region, can achieve a similar engine without
 601 going through a phase transition.

A. Acknowledgements:

602 One of the authors, MR acknowledges The Univer-
 603 sity of Burdwan for support via a state-funded fel-
 604 lowship. AR acknowledges support from the Uni-
 605 versity Grants Commission (UGC) of India, via BSR
 606 Startup Grant No. F.30-425/2018(BSR), as well as
 607 from the Science and Engineering Research Board
 608 (SERB) Core Research Grant No. CRG/2018/004002.

- [1] S. Bordia Pranjal, Lüschen Henrik, *Nature Physics* **13**, 460 (2017).
- [2] S. Sahoo, I. Schneider, and S. Eggert, *Periodically driven many-body systems: A floquet density matrix renormalization group study* (2019), arXiv:1906.00004 [cond-mat.str-el].
- [3] A. Das, *Phys. Rev. B* **82**, 172402 (2010).
- [4] G. B. Mbeng, A. Russomanno, and G. E. Santoro, *The quantum ising chain for beginners* (2020), arXiv:2009.09208 [quant-ph].
- [5] H. S. Yamada and K. S. Ikeda, *Phys. Rev. E* **105**, 054201 (2022).
- [6] A. Roy and A. Das, *Phys. Rev. B* **91**, 121106 (2015).
- [7] H. Li, B. Shapiro, and T. Kottos, *Phys. Rev. B* **98**, 121101 (2018).
- [8] A. Eckardt and E. Anisimovas, *New Journal of Physics* **17**, 093039 (2015).
- [9] L. Zhang, V. Khemani, and D. A. Huse, *Phys. Rev. B* **94**, 224202 (2016).
- [10] V. Khemani, A. Lazarides, R. Moessner, and S. L. Sondhi, *Phys. Rev. Lett.* **116**, 250401 (2016).
- [11] N. Yunger Halpern, C. D. White, S. Gopalakrishnan, and G. Refael, *Phys. Rev. B* **99**, 024203 (2019).
- [12] T. Nag, S. Roy, A. Dutta, and D. Sen, *Phys. Rev. B* **89**, 165425 (2014).
- [13] G. Carleo, F. Becca, M. Schiró, and M. Fabrizio, *Scientific Reports* **2**, 243 (2012).
- [14] S. Aditya and D. Sen, *Dynamical localization and slow thermalization in a class of disorder-free periodically driven one-dimensional interacting systems* (2023), arXiv:2305.06056 [cond-mat.stat-mech].
- [15] M. Schiulaz, A. Silva, and M. Müller, *Phys. Rev. B* **91**, 184202 (2015).
- [16] T. Grover and M. P. A. Fisher, *2014*, P10010.
- [17] Z. Papić, E. M. Stoudenmire, and D. A. Abanin, *Annals of Physics* **362**, 714 (2015).
- [18] A. Smith, J. Knolle, D. L. Kovrizhin, and R. Moessner, *Phys. Rev. Lett.* **118**, 266601 (2017).
- [19] O. Hart, S. Gopalakrishnan, and C. Castelnovo, *Phys. Rev. Lett.* **126**, 227202 (2021).
- [20] H. Lipkin, N. Meshkov, and A. Glick, *Nuclear Physics* **62**, 188 (1965).
- [21] N. Meshkov, A. Glick, and H. Lipkin, *Nuclear Physics* **62**, 199 (1965).
- [22] A. Glick, H. Lipkin, and N. Meshkov, *Nuclear Physics* **62**, 211 (1965).
- [23] P. Ribeiro, J. Vidal, and R. Mosseri, *Phys. Rev. E* **78**, 021106 (2008).
- [24] N. Debergh and F. Stancu, *Journal of Physics A: Mathematical and General* **34**, 3265 (2001).
- [25] P. Titum and M. F. Maghrebi, *Phys. Rev. Lett.* **125**, 040602 (2020).
- [26] A. Campa, T. Dauxois, and S. Ruffo, *Physics Reports* **480**, 57 (2009).
- [27] E. R. S. Eisele, *Theodor, Journal of Statistical Physics*, 161 (1988).
- [28] A. Canning, *Physica A: Statistical Mechanics and its Applications* **185**, 254 (1992).
- [29] D. Vu, K. Huang, X. Li, and S. Das Sarma, *Phys. Rev. Lett.* **128**, 146601 (2022).
- [30] G. Misguich, V. Pasquier, and J.-M. Luck, *Phys. Rev. B* **94**, 155110 (2016).
- [31] M. Calixto and E. Romera, *Journal of Statistical Mechanics: Theory and Experiment* **2015**, P06029 (2015).
- [32] K. Fujii, *Journal of Modern Physics* **8**, 2042 (2017).
- [33] B. Sutherland, *Beautiful Models* (WORLD SCIENTIFIC, 2004) Chap. 2.
- [34] D. A. Abanin, E. Altman, I. Bloch, and M. Serbyn, *Rev. Mod. Phys.* **91**, 021001 (2019).
- [35] M. Srednicki, *Phys. Rev. E* **50**, 888 (1994).
- [36] M. Srednicki, *Journal of Physics A: Mathematical and General* **32**, 1163 (1999).
- [37] M. Holthaus, *Journal of Physics B: Atomic, Molecular and Optical Physics* **49**, 013001 (2015).
- [38] M. Vogl, M. Rodriguez-Vega, and G. A. Fiete, *Phys. Rev. B* **101**, 024303 (2020).
- [39] M. Bukov, L. D'Alessio, and A. Polkovnikov, *Advances in Physics* **64**, 139 (2015).
- [40] L. D'Alessio and M. Rigol, *Phys. Rev. X* **4**, 041048 (2014).
- [41] R. Yousefjani, S. Bose, and A. Bayat, *Phys. Rev. Res.* **5**, 013094 (2023).
- [42] P. Sierant, M. Lewenstein, A. Scardicchio, and J. Zakrzewski, *Phys. Rev. B* **107**, 115132 (2023).
- [43] R. Yousefjani, S. Bose, and A. Bayat, *Phys. Rev. Res.* **5**, 013094 (2023).
- [44] F. Alet and N. Laflorencie, *Comptes Rendus Physique* **19**, 498 (2018).
- [45] S. J. Garratt and S. Roy, *Phys. Rev. B* **106**, 054309 (2022).
- [46] R. B. Stinchcombe, *Journal of Physics C: Solid State Physics* **6**, 2459 (1973).
- [47] F. E. H. George Arfken, Hans Weber, *Mathematical Methods for Physicists*, 7th ed. (Academic Press).
- [48] S. Mukherjee, A. Spracklen, D. Choudhury, N. Goldman, P. Öhberg, E. Andersson, and R. R. Thomson, *New Journal of Physics* **17**, 115002 (2015).
- [49] S.-H. Lin, B. Sbierski, F. Dorfner, C. Karrasch, and F. Heidrich-Meisner, *SciPost Phys.* **4**, 002 (2018).
- [50] N. C. Murphy, R. Wortis, and W. A. Atkinson, *Phys. Rev. B* **83**, 184206 (2011).
- [51] E. J. Torres-Herrera, I. Vallejo-Fabila, A. J. Martínez-Mendoza, and L. F. Santos, *Phys. Rev. E* **102**, 062126 (2020).
- [52] N. Trivedi and D. Heidarian, *Progress of Theoretical Physics Supplement* **160**, 296 (2005).
- [53] G. Misguich, V. Pasquier, and J.-M. Luck, *Phys. Rev. B* **94**, 155110 (2016).
- [54] A. Russomanno, R. Fazio, and G. E. Santoro, *Europhysics Letters* **110**, 37005 (2015).
- [55] N. Defenu, T. Enss, M. Kastner, and G. Morigi, *Phys. Rev. Lett.* **121**, 240403 (2018).
- [56] T. Mori, *Journal of Physics A: Mathematical and Theoretical* **52**, 054001 (2019).
- [57] J. Johansson, P. Nation, and F. Nori, *Computer Physics Communications* **184**, 1234.

- ⁷²⁶ [58] B. Sciolla and G. Biroli, Phys. Rev. Lett. **105**, 220401
⁷²⁷ (2010).
- ⁷²⁸ [59] R. A. Kidd, M. K. Olsen, and J. F. Corney, Phys. Rev. A **100**, 013625 (2019).
- ⁷³⁰ [60] A. Bäcker, S. Fürstberger, and R. Schubert, Phys. Rev. E **70**, 036204 (2004).
- ⁷³² [61] S. Sachdev, *Quantum Phase Transitions*, 2nd ed. (Cambridge University Press, Cambridge, 2011).
- ⁷³⁴ [62] P. Reimann, Journal of Statistical Mechanics: Theory and Experiment **2021**, 103106 (2021).
- ⁷³⁶ [63] When frozen, $|\psi(t)\rangle \approx |s_N\rangle$. From eqn 17, $\langle \hat{H}_{0,1} \rangle$ are
⁷³⁷ both approximately constant. Averaging the square of
⁷³⁸ $\langle \hat{H}(t) \rangle$ over long times $\tau \gg T$ yields a result that goes
⁷³⁹ as $h^2 + \delta$, where $\delta \sim h_0 \ll 1$. Thus, the standard devia-
⁷⁴⁰ tion in time will go as $\sim h \sim \omega$, since $\eta = 4h/\omega$ is kept
⁷⁴¹ fixed.
- ⁷⁴² [64] L. Reichl, *The Transition to Chaos: Conservative Clas-
⁷⁴³ sical and Quantum Systems*, Fundamental Theories of
⁷⁴⁴ Physics, Vol. 200 (Springer International Publishing).
- ⁷⁴⁵ [65] N. Srivatsa, R. Moessner, and A. E. Nielsen, Phys. Rev.
⁷⁴⁶ Lett. **125**, 240401.
- ⁷⁴⁷ [66] Quantum ising phase transition.
- ⁷⁴⁸ [67] B. Marcos, A. Gabrielli, and M. Joyce, Open Physics **10**,
⁷⁴⁹ 676.
- ⁷⁵⁰ [68] A. Haldar and A. Das, Annalen der Physik **529**,
⁷⁵¹ 1600333.
- ⁷⁵² [69] J. M. Deutsch, Phys. Rev. A **43**, 2046 () .
- ⁷⁵³ [70] E. W. Hobson, On the Second Mean-Value Theorem of
⁷⁵⁴ the Integral Calculus (1909).
- ⁷⁵⁵ [71] M. Rigol and M. Srednicki, Physical Review Letters
⁷⁵⁶ **108**, 10.1103/physrevlett.108.110601 (2012).
- ⁷⁵⁷ [72] J. M. Deutsch, IOP Publishing Ltd **81**, 296 () .
- ⁷⁵⁸ [73] R. Nandkishore and D. A. Huse, Annual Re-
⁷⁵⁹ view of Condensed Matter Physics **6**, 15 (2015),
⁷⁶⁰ <https://doi.org/10.1146/annurev-conmatphys-031214-014726>.
- ⁷⁶² [74] L. D'Alessio and A. Polkovnikov, **333**, 19.
- ⁷⁶³ [75] S. Notarnicola, F. Iemini, D. Rossini, R. Fazio, A. Silva,
⁷⁶⁴ and A. Russomanno, Phys. Rev. E **97**, 022202 (2018).
- ⁷⁶⁵ [76] A. Lazarides, A. Das, and R. Moessner, Phys. Rev. Lett.
⁷⁶⁶ **115**, 030402 (2015).